

Superconductivity in type-II Weyl-semimetal WTe_2 induced by a normal metal contact

Artem Kononov,^{1,*} Martin Endres,¹ Gulibusitan Abulizi,¹ Kejian Qu,² Jiaqiang Yan,^{3,2} David G. Mandrus,^{2,3} Kenji Watanabe,⁴ Takashi Taniguchi,⁴ and Christian Schönenberger^{1,5,†}

¹*Department of Physics, University of Basel, Klingelbergstrasse 82, CH-4056 Basel, Switzerland*

²*Department of Materials Science and Engineering, University of Tennessee, Knoxville, TN 37996, United States*

³*Materials Science and Technology Division, Oak Ridge National Laboratory, Oak Ridge, TN 37831, United States*

⁴*National Institute for Material Science, 1-1 Namiki, Tsukuba 305-0044, Japan*

⁵*Swiss Nanoscience Institute, University of Basel, Klingelbergstrasse 82, CH-4056 Basel, Switzerland*

WTe_2 is a material with rich topological properties: it is a 2D topological insulator as a monolayer and a Weyl-semimetal and higher-order topological insulator (HOTI) in the bulk form. Inducing superconductivity in topological materials is a way to obtain topological superconductivity, which lays at the foundation for many proposals of fault tolerant quantum computing. Here, we demonstrate the emergence of superconductivity at the interface between WTe_2 and the normal metal palladium. The superconductivity has a critical temperature of about 1.2 K. By studying the superconductivity in perpendicular magnetic field, we obtain the coherence length and the London penetration depth. These parameters correspond to a low Fermi velocity and a high density of states at the Fermi level. This hints to a possible origin of superconductivity due to the formation of flat bands. Furthermore, the critical in-plane magnetic field exceeds the Pauli limit, suggesting a non-trivial nature of the superconducting state.

INTRODUCTION

Topological materials attract a lot of attention in modern condensed matter physics. This interest stems from intriguing fundamental properties and great potential for practical applications. The especially interesting class of topological materials are topological superconductors, promising to revolutionize quantum computing due to the inherent error protection [1]. Topological superconductivity could be obtained by inducing superconductivity in topologically non-trivial system. There are several theoretical predictions of different topological superconducting states in Dirac and Weyl semimetal based systems, including Fulde–Ferrell–Larkin–Ovchinnikov superconductors [2–4], the time-reversal invariant topological superconductor [5], chiral non-Abelian Majorana fermions [6], and flat band superconductivity [7].

WTe_2 is a layered transition-metal dichalcogenide with rich topological properties. As a bulk material it is a type-II Weyl semimetal with bulk Weyl nodes connected by Fermi arcs surface states [8, 9]. Recently, it has been predicted to be a higher-order topological insulator with one-dimensional hinge states [10], experimental evidence of these states has been obtained [11–13]. In a single layer form, WTe_2 is a two-dimensional topological insulator with helical edge states [14, 15]. In addition to all these topological phases WTe_2 has a tendency of becoming superconducting under different conditions: under pressure [16, 17], electron doping [18] or electrostatic gating [19, 20]. The combination of these properties makes WTe_2 a particularly promising candidate for topological superconductivity.

In this manuscript we demonstrate the emergence of superconductivity at the interface between the normal metal palladium and few-layer thick WTe_2 . Studying

the transport properties in magnetic field and at different temperatures we deduce the main parameters characterizing the superconducting state including the critical temperature, the coherence length and the London penetration depth. These parameters correspond to a low Fermi velocity and a high density of states at the Fermi level. This hints to a possible origin of superconductivity due to the formation of flat bands. Moreover, the measured in-plane critical field exceeds the Pauli limit, suggesting non-trivial superconducting pairing. The coexistence of the observed superconductivity with topological states in WTe_2 makes it a promising platform for studying topological superconductivity and applications for quantum computing.

EXPERIMENT

The single crystals of WTe_2 were grown with a flux growth method [21]. We obtained few-layer thick WTe_2 flakes by mechanically exfoliating single crystals with an adhesive tape on oxidized Si substrate with 295 nm SiO_2 layer. To avoid oxidation of WTe_2 , the exfoliation has been carried out in a glovebox with low oxygen content. We selected few-layer thick (5-12 single layers) stripe shaped flakes. Suitable flakes have been identified with an optical contrast method [22] and were picked up and transferred using the polycarbonate assisted pick-up technique [23] on the device chip that already contained prepatterned contacts. The contacts were defined before using standard e-beam lithography and metal deposition of 3 nm titanium and 12 nm palladium. In the final stack WTe_2 is protected from oxidation by an hBN layer that covers the WTe_2 . All the measurements were performed in a dilution refrigerator with a base temperature of 60 mK. Similar superconducting properties have

been observed in multiple devices, data presented in the manuscript were collected from 3 samples.

RESULTS AND DISCUSSION

Fig. 1(a) shows an optical image of an encapsulated WTe₂ crystal with a contact pattern that resembles a standard Hall-bar configuration. Note, that the visible Pd contacts are at the bottom, followed by a few layer WTe₂ crystal with a rectangular shape and high-aspect ratio oriented vertically, followed by an hBN layer that has the weakest contrast in the image. The drawn electrical schematics corresponds to the measurement of the longitudinal resistance R_{xx} given by V_{xx}/I .

Fig. 1(b) displays R_{xx} as a function of perpendicular magnetic field B_{\perp} . At 4 K the resistance shows a non-saturating magnetoresistance characteristic for WTe₂ [24]. The small thickness (7 layers) of our WTe₂ crystal results in a relatively small magnetoresistance [25]. Another evidence of the high quality of our samples is the presence of Shubnikov–de Haas oscillations at low temperature. The frequency of the oscillations $f_{1/B} \sim 100$ T corresponds to an electron density $n_{2D} = e/(\pi\hbar f_{1/B}) \sim 5 \cdot 10^{12} \text{ cm}^{-2}$ and Fermi wavevector $k_F = \sqrt{\pi n_{2D}} \sim 0.4 \text{ nm}^{-1}$ (here the two electron pockets of WTe₂ are taken into account). The oscillations visibility at around 5 T suggest a mobility of at least $2000 \text{ cm}^2 \text{ V}^{-1} \text{ s}^{-1}$, which yields an electron mean free path of $l_{mfp} = k_F \hbar \mu / e \sim 50 \text{ nm}$.

At low temperature additional features develop in $R_{xx}(B_{\perp})$: at zero field the resistance goes to zero and in small fields it has an intermediate state between zero and high-temperature values. The asymmetry in $R_{xx}(B)$ is defined by the sweep direction and rate, thus it is likely connected with heating during the magnetic field sweep. The intermediate resistance state in Fig. 1(b) is a result of the formation of a superconducting state in WTe₂ above the Pd leads. Furthermore, these superconducting regions could be connected by the Josephson effect, as illustrated in Fig. 1(c), leading to a zero longitudinal resistance. The zero resistance state appears only for smaller distances between the contacts, excluding intrinsic superconductivity in our WTe₂ samples. This explanation is further supported by $R_{xx}(T)$ dependence in Fig. 1(d). With decreasing temperature the first superconducting transition takes place in the range 1.05–1.2 K, followed by the gradual developing of the Josephson effect at lower temperature achieving zero resistance below 350 mK.

To understand the properties of the superconducting state we studied the evolution of $R_{xx}(B_{\perp})$ with increasing temperature, as shown in Fig. 2(a). Upon temperature increase both transitions in the resistance are shifting towards zero field. The zero resistance state connected to the Josephson coupling disappears first above 0.75 K, the second transition connected to the suppres-

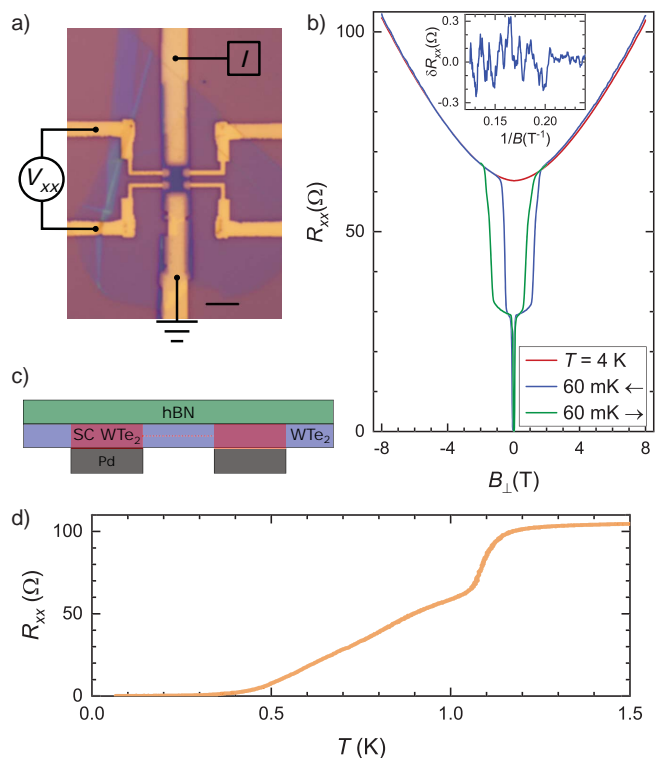


FIG. 1. (a) Optical image of sample 1 (scale bar 5 μm) with a sketch of the measurement setup. (b) Longitudinal resistance $R_{xx} = V_{xx}/I$ as a function of perpendicular magnetic field B_{\perp} . At 4 K only a non-saturating magnetoresistance is seen, whereas at 60 mK the resistance shows additionally a transition to a smaller value in a magnetic field of $B_{\perp} \sim 1$ T and a transition to zero-resistance due to emerging superconductivity for much lower B_{\perp} . The asymmetry in $R_{xx}(B)$ is likely connected with heating during magnetic field sweep, since it depends on the sweep direction and gets reduced with lower sweep rate. Inset: Shubnikov–de Haas oscillations highlighted by subtracting the overall quadratic trend from the 60 mK curve. (c) Cross-sectional view through the contact region: The region of WTe₂ above the Pd leads turn into superconducting regions (red). These regions can be connected by the Josephson effect (red dashed line) if not too far apart. (d) Longitudinal resistance R_{xx} as a function of temperature. Superconducting transition takes place in the range 1.05–1.2 K. The Josephson effect gradually develops at lower temperature achieving zero resistance state below 350 mK. Panels (a) and (c) reprinted with permission from A. Kononov *et al.*, Nano Lett. **20**, 4228 (2020) (<https://pubs.acs.org/doi/10.1021/acs.nanolett.0c00658>). Copyright 2020, American Chemical Society. Further permission related to the material excerpted should be directed to the ACS.

sion of superconductivity by magnetic field B_{c2} persists up to 1.1 K. We define $B_{c2}(T)$ as the magnetic field where the $R_{xx}(B_{\perp})$ crosses the fixed resistance value $R_{xx} = 45 \text{ } \Omega$, which approximately corresponds to half of the resistance step. Fig. 2(b) shows the extracted dependence of the critical magnetic field as a function of temperature T . The $B_{c2}(T)$ dependence is linear as ex-

pected for a 2D superconductor

$$B_{c2}(T) = \frac{\Phi_0}{2\pi\xi_{GL}^2} \left(1 - \frac{T}{T_c}\right), \quad (1)$$

where Φ_0 is the magnetic flux quantum, ξ_{GL} is the Ginzburg-Landau coherence length at zero temperature, and T_c is the critical temperature at zero magnetic field. Fitting the experimental data with equation 1, we obtain $T_c \sim 1.2$ K and relatively short $\xi_{GL} \sim 14$ nm.

Disorder can cause the reduction of the coherence length, but we don't think this is the case in our samples, since we have found $l_{mfp} > \xi$ and non-saturating magnetoresistance. In the clean limit at low temperatures the Ginzburg-Landau coherence length is similar to the Bardeen-Cooper-Schrieffer (BCS) coherence length $\xi_{GL} \sim \xi$. Knowing the coherence length and the critical temperature, we can estimate the Fermi velocity $v_F = \xi\pi\Delta/\hbar$, where we take for $\Delta(T_c)$ the BCS relation $\Delta \sim 1.76k_B T_c$, yielding $v_F \sim 1.2 \cdot 10^4$ m s⁻¹. The obtained small value of Fermi velocity could suggest superconductivity due to the formation of flat bands [26].

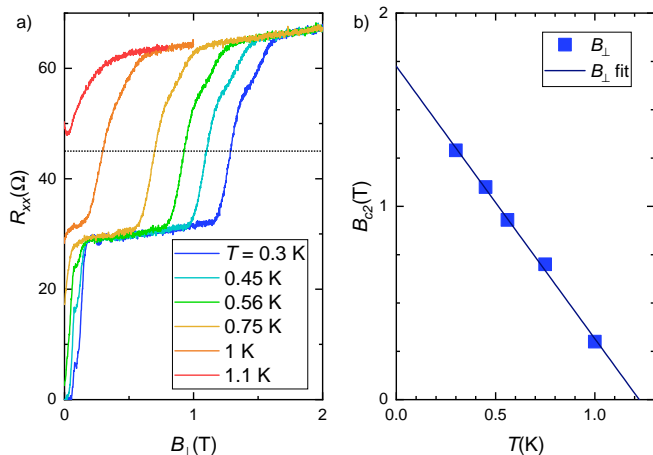


FIG. 2. (a) Longitudinal resistance as a function of perpendicular magnetic field B_{\perp} at different temperatures. The dotted line indicates the resistance value used to determine $B_{c2}(T)$. The increase in the resistance near $B_{\perp} = 0$ is connected with heating of the sample during field sweeps. (b) Critical magnetic field B_{c2} as function of temperature extracted from (a) and a $B_{c2} \propto (1 - T/T_c)$ fit of the data. Panel (a) reprinted with permission from A. Kononov *et al.*, *Nano Lett.* **20**, 4228 (2020) (<https://pubs.acs.org/doi/10.1021/acs.nanolett.0c00658>). Copyright 2020, American Chemical Society. Further permission related to the material excerpted should be directed to the ACS.

We further investigate the superconducting properties by looking at the R_{xx} dependence on the *in-plane* magnetic field B_{\parallel} , as shown in Fig. 3(a). Compared with the perpendicular field, both changes in the resistance have shifted to higher magnetic fields. We extracted the critical field values as a function of temperature and plotted them in Fig. 3(b). In this case,

$B_{c2}(T)$ follows the known empirical law for superconductors $B_{c2}(T) = B_{c2}(0) [1 - (T/T_c)^2]$ [27], as evident from the very good agreement between measured points and the fit. Both fits of the critical field as a function of B_{\perp} and B_{\parallel} converge to the same temperature $T_c \sim 1.2$ K.

A notable feature of the parallel critical field is its large value, which exceeds the Pauli paramagnetic limit B_P . The latter is given by $B_P \sim 1.76k_B T_c \sqrt{2}/g\mu_B \sim 1.86T_c \sim 2.3$ T. This expression is based on the BCS theory for weak-coupling superconductors and a free electron g -factor of $g = 2$ [28]. This effect has also been observed in gated monolayer [19, 20] and doped bulk WTe_2 [18], and ultrathin films of other materials [29, 30]. Several mechanisms could be responsible for superconductivity exceeding the Pauli limit, including Ising-type superconductivity [28] or a diminishing of the effective g -factor due to strong spin-orbit coupling [31]. Further studies are required to resolve this.

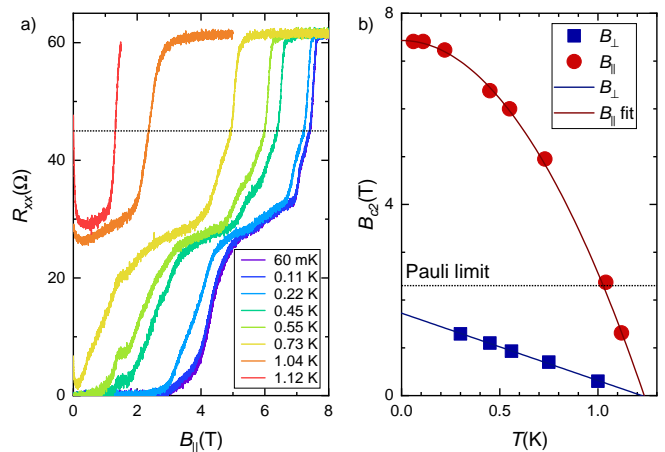


FIG. 3. (a) Longitudinal resistance as a function of in-plane magnetic field at different temperatures. The dotted line indicates the resistance level used to determine $B_{c2}(T)$. The increase in the resistance near $B_{\parallel} = 0$ is connected with heating of the sample during field sweeps. (b) Critical magnetic field as function of temperature extracted from (a) and fit to the data. The dotted line indicates the maximum critical field given by the Pauli limit B_P , which we estimate to 2.3 T. The data for the critical perpendicular magnetic field is shown for comparison.

The London penetration depth λ_L is another important characteristic of a superconductor. While RF-measurements are a common way of measuring the penetration depth [32], it can also be estimated by measuring the critical current of a Josephson junction in a magnetic field B_{\perp} . A Josephson junction placed in a perpendicular magnetic field demonstrates an oscillating critical current. One period of the oscillations corresponds to the magnetic flux quantum Φ_0 through the effective area of the junction $S_{eff} = WL_{eff} = W(L + 2\lambda)$, where W and L are the junction's width and length, respectively, and λ is the magnetic field penetration depth [27], see Fig 4(a).

For a bulk superconductor $\lambda = \lambda_L$, but for a thin film superconductor with thickness d , the penetration depth is a function of the thickness $\lambda(d) = \lambda_L \coth(d/\lambda_L)$ [32]. In the limit of small thickness $d \ll \lambda_L$ the previous expression is equal to the Pearl's penetration depth $\lambda_P = \lambda_L^2/d$.

Fig. 4(b) demonstrates several examples of $I_c(B_\perp)$ dependencies for Josephson junctions in WTe₂ where the superconducting regions on top of Pd play the role of superconducting contacts. These dependencies have a SQUID-like character due to hinge states [11] with a rapidly decaying Fraunhofer contribution due to the Fermi-arc surface states [33, 34] or the bulk conductivity. The SQUID-like oscillations with many visible periods allow to determine the period with a high precision. For junctions 1 and 2, with $L = 1 \mu\text{m}$ and $W = 4.3 \mu\text{m}$, we obtain a period of $\Delta B = 0.27 \text{ mT}$. This period corresponds to $L_{eff} = 1.77 \mu\text{m}$ and a penetration depth of $\lambda = 380 \text{ nm}$. For junction 3 ($L = 500 \text{ nm}$, $W = 4.2 \mu\text{m}$) we obtain $\Delta B = 0.41 \text{ mT}$, yielding $\lambda = 350 \text{ nm}$. The obtained penetration depth is much larger than the thickness of the WTe₂ flakes $d \sim 7 \text{ nm}$ (approximately 10-layers thick) so that the extracted penetration depth is given by Pearl's limit $\lambda = \lambda_P = \lambda_L^2/d$. Using this expression we estimate the London penetration depth to be $\lambda_L \sim 50 \text{ nm}$. The ratio between the London penetration depth and the coherence length $\kappa = \lambda_L/\xi$ is $\kappa \sim 3 > 1/\sqrt{2}$, suggesting type-II superconductivity [27].

The obtained London penetration depth is comparable to typical values for metals and is surprisingly small considering the semimetallic nature of WTe₂. This additionally speaks against the presence of disorder in our samples, since the penetration depth is expected to be higher in dirty superconductors [27]. An estimate of the superconducting electron density yields a quite high value $n_s = m/\mu_0\lambda_L^2 e^2 \sim 3 \cdot 10^{21} \text{ cm}^{-3}$, where $m \sim 0.3m_e$ is the effective mass of the electrons in WTe₂ [35]. This value is higher than the typical carrier densities in WTe₂ $n \sim 10^{19} \text{ cm}^{-3}$ [36] and corresponds to a density per single layer of $n_s^{1L} \sim 2 \cdot 10^{14} \text{ cm}^{-2}$, which is an order of magnitude higher than the electron density in monolayer WTe₂ with gate induced superconductivity [19, 20], but comparable to the predicted optimal charge carrier density [37]. Furthermore, a large superconducting carrier density implies a high density of states at the Fermi level $g(E_F) \sim n_s/2\Delta \sim 8 \cdot 10^{24} \text{ cm}^{-3} \text{ eV}^{-1}$, which is a signature of flat bands.

The emergence of superconductivity at the interface of two non-superconducting materials is quite surprising, despite the fact that it has been observed previously in different Weyl and Dirac semimetals [38–42]. While the underlying mechanism for the superconductivity is unclear, in our case of WTe₂/Pd interface several material specific reasons for the superconductivity could be proposed. First, the structural change at the interface could lead to the superconductivity similar to the pressure induced superconductivity in WTe₂ [16, 17]. Sec-

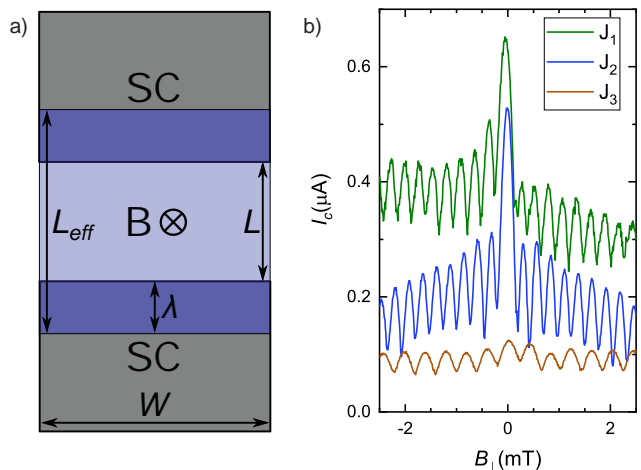


FIG. 4. (a) Illustration of flux focusing in Josephson junction. The area of the junction, where the magnetic field is not screened and penetrating the junction, is given by an effective area $W \times L_{eff}$, rather than the geometrical area $W \times L$, where L is the junction length. Here, the effective length L_{eff} equals $L + 2\lambda$, where λ is accounting for the penetration depth of the field into the superconductor. (b) Critical current as a function of magnetic field for three different Josephson junctions. Junctions J₁ and J₂ have $W = 4.3 \mu\text{m}$ and length $L = 1 \mu\text{m}$ and junction J₃ has $W = 4.2 \mu\text{m}$, $L = 500 \text{ nm}$. Data in (b) used with permission from A. Kononov *et al.*, Nano Lett. **20**, 4228 (2020) (<https://pubs.acs.org/doi/10.1021/acs.nanolett.0c00658>). Copyright 2020, American Chemical Society. Further permission related to the material excerpted should be directed to the ACS.

ond, electron doping from palladium [43] could create a superconducting state similar to what was seen in monolayer [19, 20] or bulk doped WTe₂ [18]. The latter seems to be the more probable explanation, since the in-plane critical field exceeds the Pauli limit, which has been observed in doped WTe₂ [18–20], but not in the pressure induced superconductivity [16, 17]. Another possibility is interdiffusion of Pd and Te with a formation of superconducting PdTe₂, which has been recently reported in samples with Pd deposited on $(\text{Bi}_{1-x}\text{Sb}_x)_2\text{Te}_3$ [44]. We think that this mechanism is unlikely in our case, since WTe₂ and Pd are merely placed in contact by stacking and the samples were never heated above 180°C.

Even more intriguing is the possibility of the flat band superconductivity [45, 46], as suggested by the small Fermi velocity and high density of states at the Fermi level. Flat bands are ubiquitous in van der Waals (vdW) heterostructures. For example, high carrier-density combined with a low Fermi velocity has been observed close to van-Hove singularities in the band structure of superlattices formed in hBN-encapsulated graphene [47]. And the presence of the flat bands is known to stimulate superconductivity [26, 48, 49].

Establishing the presence of the flat band superconductivity at WTe₂/Pd interface and understanding the

reasons for it will require further experiments, but some explanations could be outlined already. Flat band superconductivity can be formed as the result of a topological phase transition due to strain at the interface [7, 46]. Furthermore, flat band superconductivity has been observed in vdW systems with moiré pattern [26]. This possibility is feasible since the mismatch between lattice constant in Pd (0.389 nm [50]) and a-axis lattice constant in WTe₂ (0.349nm [17]) is only about 10%. But we deem this scenario unlikely, since moiré patterns strongly depend on the mutual orientation of the lattices, while we observe superconductivity in multiple samples without any intentional alignment of the lattices.

An alternative explanation for the experimental data could be a multiband superconductivity in our samples. In this situation a sublinear dependence of $B_{c2}^{\perp}(T)$ and exceeding Pauli limit by B_{c2}^{\parallel} could be expected in the dirty limit of the superconductivity [51], which seems not to be the case in our samples.

CONCLUSION

We demonstrate the emergence of superconductivity at the interface between type-II Weyl semimetal WTe₂ and normal metal palladium. Studying the transport properties in magnetic field and at different temperatures we deduce the key parameters that characterize the superconducting state, including the critical temperature T_c , the coherence length ξ and the London penetration depth λ_L . The combined set of parameters hint to a possible origin of superconductivity being due to the formation of flat bands. Moreover, the measured in-plane critical field exceeds the Pauli limit, suggesting non-trivial superconducting pairing. The coexistence of superconductivity with topological states makes WTe₂ a promising platform for topological superconductivity and applications for quantum computing.

ACKNOWLEDGMENTS

We thank A. Baumgartner for helpful discussions. A.K. was supported by the Georg H. Endress foundation. This project has received further funding from the European Research Council (ERC) under the European Union's Horizon 2020 research and innovation programme: grant agreement No 787414 TopSupra, by the Swiss National Science Foundation through the National Centre of Competence in Research Quantum Science and Technology (QSIT), and by the Swiss Nanoscience Institute (SNI). K.W. and T.T. acknowledge support from the Elemental Strategy Initiative conducted by MEXT, Japan and the CREST (JPMJCR15F3), JST. D.G.M. and J.Y. acknowledge support from the U.S. Department of Energy (U.S.-DOE), Office of Science - Basic Energy

Sciences (BES), Materials Sciences and Engineering Division. D.G.M. acknowledges support from the Gordon and Betty Moore Foundation's EPIQS Initiative, Grant GBMF9069.

DATA AVAILABILITY

All data in this publication are available in numerical form in the Zenodo repository at <https://doi.org/10.5281/zenodo.3934679> [52].

* Artem.Kononov@unibas.ch

† Christian.Schoenenberger@unibas.ch

- [1] S. Nayak, S.H. Simon, A. Stern, M. Freedman, and S.D. Sarma, Non-Abelian anyons and topological quantum computation. *Rev. Mod. Phys.* **80**, 1083 (2008).
- [2] G.Y. Cho, J.H. Bardarson, Y.M. Lu, and J.E. Moore, Superconductivity of doped Weyl semimetals: finite-momentum pairing and electronic analog of the 3He-A phase. *Phys. Rev. B* **86**, 214514 (2012).
- [3] H.Z. Wei, S.P. Chao, and V. Aji, Odd-parity superconductivity in Weyl semimetals. *Phys. Rev. B* **89**, 014506 (2014).
- [4] G. Bednik, A.A. Zyuzin, and A.A. Burkov, Superconductivity in Weyl metals. *Phys. Rev. B* **92**, 035153 (2015).
- [5] P. Hosur, X. Dai, Z. Fang, and X.L. Qi, Time-reversal-invariant topological superconductivity in doped Weyl semimetals. *Phys. Rev. B* **90**, 045130 (2014).
- [6] C. Chan and X.J. Liu, Non-Abelian Majorana modes protected by an emergent second Chern number. *Phys. Rev. Lett.* **118**, 207002 (2017).
- [7] E. Tang and L. Fu, Strain-induced partially flat band, helical snake states and interface superconductivity in topological crystalline insulators. *Nat. Phys.* **10**, 964 (2014).
- [8] A.A. Soluyanov, D. Gresch, Z. Wang, Q.S. Wu, M. Troyer, X. Dai, and B.A. Bernevig, Type-II Weyl semimetals. *Nature* **527**, 495–498 (2015).
- [9] P. Li, Y. Wen, X. He, Q. Zhang, C. Xia, Z.-M. Yu, S.A. Yang, Z. Zhu, H.N. Alshareef, and X.-X. Zhang, Evidence for topological type-II Weyl semimetal WTe₂. *Nat. Commun.* **8**, 2150 (2017).
- [10] Z. Wang, B.J. Wieder, J. Li, B. Yan, and B.A. Bernevig, Higher-Order Topology, Monopole Nodal Lines, and the Origin of Large Fermi Arcs in Transition Metal Dichalcogenides XTe₂ (X=Mo,W). *Phys. Rev. Lett.* **123**, 186401 (2019).
- [11] A. Kononov, G. Abulizi, K. Qu, J. Yan, D. Mandrus, K. Watanabe, T. Taniguchi, and C. Schönerberger, One-Dimensional Edge Transport in Few-Layer WTe₂. *Nano Lett.* **20**, 4228 (2020).
- [12] Y.-B. Choi, Y. Xie, C.-Z. Chen, J. Park, S.-B. Song, J. Yoon, B.J. Kim, T. Taniguchi, K. Watanabe, J. Kim, K.C. Fong, M.N. Ali, K.T. Law, and G.-H. Lee, Evidence of Higher Order Topology in Multilayer WTe₂ from Josephson Coupling through Anisotropic Hinge States. *Nat. Mater.* **19**, 974 (2020).
- [13] C. Huang, A. Narayan, E. Zhang, X. Xie, L. Ai, S. Liu, C. Yi, Y. Shi, S. Sanvito, and F. Xiu, Edge superconduc-

- tivity in Multilayer WTe₂ Josephson junction. *Natl. Sci. Rev.* **7**, 1468 (2020).
- [14] Z. Fei, T. Palomaki, S. Wu, W. Zhao, X. Cai, B. Sun, P. Nguyen, J. Finney, X. Xu, and D.H. Cobden, Edge conduction in monolayer WTe₂. *Nat. Phys.* **13**, 677 (2017).
- [15] S. Wu, V. Fatemi, Q.D. Gibson, K. Watanabe, T. Taniguchi, R.J. Cava, and P. Jarillo-Herrero, Observation of the quantum spin Hall effect up to 100 Kelvin in a monolayer crystal. *Science* **359**, 76 (2018).
- [16] D. Kang, Y. Zhou, W. Yi, C. Yang, J. Guo, Y. Shi, S. Zhang, Z. Wang, C. Zhang, S. Jiang, A. Li, K. Yang, Q. Wu, G. Zhang, L. Sun, and Z. Zhao, Superconductivity emerging from a suppressed large magnetoresistant state in tungsten ditelluride. *Nat. Commun.* **6**, 7804 (2015).
- [17] X.-C. Pan, X. Chen, H. Liu, Y. Feng, Z. Wei, Y. Zhou, Z. Chi, L. Pi, F. Yen, F. Song, X. Wan, Z. Yang, B. Wang, G. Wang, and Y. Zhang, Pressure-driven dome-shaped superconductivity and electronic structural evolution in tungsten ditelluride. *Nat. Commun.* **6**, 7805 (2015).
- [18] T. Asaba, Y. Wang, G. Li, Z. Xiang, C. Tinsman, L. Chen, S. Zhou, S. Zhao, D. Laleyan, Y. Li, Z. Mi, and L. Li, Magnetic Field Enhanced Superconductivity in Epitaxial Thin Film WTe₂. *Sci. Rep.* **8**, 6520 (2018).
- [19] E. Sajadi, T. Palomaki, Z. Fei, W. Zhao, P. Bement, C. Olsen, S. Luescher, X. Xu, J.A. Folk, and D.H. Cobden, Gate-induced superconductivity in a monolayer topological insulator. *Science* **362**, 922 (2018).
- [20] V. Fatemi, S. Wu, Y. Cao, L. Bretheau, Q.D. Gibson, K. Watanabe, T. Taniguchi, R.J. Cava, P. Jarillo-Herrero, Electrically tunable low-density superconductivity in a monolayer topological insulator. *Science* **362**, 926 (2018).
- [21] Y. Zhao, H. Liu, J. Yan, W. An, J. Liu, X. Zhang, H. Wang, Y. Liu, H. Jiang, Q. Li, Y. Wang, X.-Z. Li, D. Mandrus, X.C. Xie, M. Pan, and J. Wang, Anisotropic magnetotransport and exotic longitudinal linear magnetoresistance in WTe₂ crystals. *Phys. Rev. B* **92**, 041104(R) (2015).
- [22] P. Blake, E.W. Hill, A.H. Castro Neto, K.S. Novoselov, D. Jiang, R. Yang, T.J. Booth, and A.K. Geim, Making graphene visible. *Appl. Phys. Lett.* **91**, 063124 (2007).
- [23] P.J. Zomer, M.H.D. Guimaraes, J.C. Brant, N. Tombros, and B.J. van Wees, Fast pick up technique for high quality heterostructures of bilayer graphene and hexagonal boron nitride. *Appl. Phys. Lett.* **105**, 013101 (2014).
- [24] M.N. Ali, L. Schoop, J. Xiong, S. Flynn, Q. Gibson, M. Hirschberger, N.P. Ong, and R.J. Cava, Correlation of crystal quality and extreme magnetoresistance of WTe₂. *EPL* **110**, 67002 (2015).
- [25] F.-X. Xiang, A. Srinivasan, Z.Z. Du, O. Klochan, S.-X. Dou, A.R. Hamilton, and X.-L. Wang, Thickness-dependent electronic structure in WTe₂ thin films. *Phys. Rev. B* **98**, 035115 (2018).
- [26] Y. Cao, V. Fatemi, A. Demir, S. Fang, S.L. Tomarken, J.Y. Luo, J.D. Sanchez-Yamagishi, K. Watanabe, T. Taniguchi, E. Kaxiras, R.C. Ashoori, and P. Jarillo-Herrero, Correlated insulator behaviour at half-filling in magic-angle graphene superlattices. *Nature (London)* **556**, 80 (2018).
- [27] M. Tinkham, Introduction to superconductivity second edition. (McGraw-Hill, Inc., New York, 1996).
- [28] Y. Saito, T. Nojima, Y. Iwasa, Highly crystalline 2D superconductors. *Nat. Rev. Mater.* **2**, 16094 (2016).
- [29] Y. Liu, Y. Xu, J. Sun, C. Liu, Y. Liu, C. Wang, Z. Zhang, K. Gu, Y. Tang, C. Ding, H. Liu, H. Yao, X. Lin, L. Wang, Q.-K. Xue, and J. Wang, Type-II Ising Superconductivity and Anomalous Metallic State in Macro-Size Ambient-Stable Ultrathin Crystalline Films. *Nano Lett.* **20**, 5728 (2020).
- [30] Y. Liu, Z. Wang, X. Zhang, C. Liu, Y. Liu, Z. Zhou, J. Wang, Q. Wang, Y. Liu, C. Xi, M. Tian, H. Liu, J. Feng, X.C. Xie, and J. Wang, Interface-Induced Zeeman-Protected Superconductivity in Ultrathin Crystalline Lead Films. *Phys. Rev. X* **8**, 021002 (2018).
- [31] R.A. Klemm, A. Luther, M.R. Beasley, Theory of the upper critical field in layered superconductors. *Phys. Rev. B* **12**, 877 (1975).
- [32] A.I. Gubin, K.S. Il'in, S.A. Vitusevich, M. Siegel, and N. Klein, Dependence of magnetic penetration depth on the thickness of superconducting Nb thin films. *Phys. Rev. B* **72**, 064503 (2005).
- [33] O.O. Shvetsov, A. Kononov, A.V. Timonina, N.N. Kolesnikov, and E.V. Deviatov, Realization of a Double-Slit SQUID Geometry by Fermi Arc Surface States in a WTe₂ Weyl Semimetal. *JETP Lett.* **107**, 774 (2018).
- [34] A. Kononov, O.O. Shvetsov, S.V. Egorov, A.V. Timonina, N.N. Kolesnikov, and E.V. Deviatov, Signature of Fermi arc surface states in Andreev reflection at the WTe₂ Weyl semimetal surface. *EPL* **122**, 27004 (2018).
- [35] V. Fatemi, Q.D. Gibson, K. Watanabe, T. Taniguchi, R.J. Cava, and P. Jarillo-Herrero, Magnetoresistance and quantum oscillations of an electrostatically tuned semimetal-to-metal transition in ultrathin WTe₂. *Phys. Rev. B* **95**, 041410(R) (2017).
- [36] Z. Zhu, X. Lin, J. Liu, B. Fauqué, Q. Tao, C. Yang, Y. Shi, and K. Behnia, Quantum oscillations, thermoelectric coefficients, and the Fermi surface of semimetallic WTe₂. *Phys. Rev. Lett.* **114**, 176601 (2015).
- [37] W. Yang, C.-J. Mo, S.-B. Fu, Y. Yang, F.-W. Zheng, X.-H. Wang, Y.-A. Liu, N. Hao, and P. Zhang, Soft-mode-phonon-mediated unconventional superconductivity in monolayer 1T'-WTe₂. *Phys. Rev. Lett.* **125**, 237006 (2020).
- [38] L. Aggarwal, A. Gaurav, G.S. Thakur, Z. Haque, A.K. Ganguli, and G. Sheet, Unconventional superconductivity at mesoscopic point contacts on the 3D Dirac semimetal Cd₃As₂. *Nat. Mat.* **15**, 32 (2016).
- [39] H. Wang, H. Wang, H. Liu, H. Lu, W. Yang, S. Jia, X.-J. Liu, X.C. Xie, J. Wei, and J. Wang, Observation of superconductivity induced by a point contact on 3D Dirac semimetal Cd₃As₂ crystals. *Nat. Mat.* **15**, 38 (2016).
- [40] O.O. Shvetsov, V.D. Esin, A.V. Timonina, N.N. Kolesnikov, and E.V. Deviatov, Surface superconductivity in three-dimensional Cd₃As₂ semimetal at the interface with a gold contact. *Phys. Rev. B* **99**, 125305 (2019).
- [41] W. Zhu, X. Hou, J. Li, Y. Huang, S. Zhang, J. He, D. Chen, Y. Wang, Q. Dong, M. Zhang, H. Yang, Z. Ren, J. Hu, L. Shan, G. Chen, Interfacial superconductivity on the topological semimetal tungsten carbide induced by metal deposition. *Adv. Mater.* **32**, 1907970 (2020).
- [42] Y. Xing, Z. Shao, J. Ge, J. Luo, J. Wang, Z. Zhu, J. Liu, Y. Wang, Z. Zhao, J. Yan, D. Mandrus, B. Yan, X.-J. Liu, M. Pan, J. Wang, Surface superconductivity in the type

- II Weyl semimetal TaIrTe₄. *Nat. Sc. Rev.* **7**, 579, (2020).
- [43] B. Shao, A. Eich, C. Sanders, A.S. Ngankeu, M. Bianchi, P. Hofmann, A.A. Khajetoorians, and T.O. Wehling, Pseudodoping of a metallic two-dimensional material by the supporting substrate. *Nat. Commun.* **10**, 180 (2019).
- [44] M. Bai, F. Yang, M. Luysberg, J. Feng, A. Bliesener, G. Lippertz, A.A. Taskin, J. Mayer, and Y. Ando, Novel self-epitaxy for inducing superconductivity in the topological insulator (Bi_{1-x}Sb_x)₂Te₃. *Phys. Rev. Mat.* **4**, 094801 (2020).
- [45] M. Alidoust, K. Halterman, and A.A. Zyuzin, Superconductivity in type-II Weyl semimetals. *Phys. Rev. B* **95**, 155124 (2017).
- [46] V.J. Kauppila, F. Aikebaier, and T.T. Heikkilä, Flat-band superconductivity in strained Dirac materials. *Phys. Rev. B* **93**, 214505 (2016).
- [47] D.I. Indolese, R. Delagrance, P. Makk, J.R. Wallbank, K. Watanabe, T. Taniguchi, and C. Schönberger, Signatures of van Hove singularities probed by the supercurrent in a graphene – hBN superlattice. *Phys. Rev. Lett.* **121**, 137701 (2018).
- [48] Yu.S. Barash and P.I. Nagornykh, Dispersionless modes and the superconductivity of ultrathin films. *JETP Lett.* **83**, 376 (2006).
- [49] N.B. Kopnin, T.T. Heikkilä, and G.E. Volovik, High-temperature surface superconductivity in topological flat-band systems. *Phys. Rev. B* **83**, 220503(R) (2011).
- [50] W.P. Davey, Precision measurements of the lattice constants of twelve common metals. *Phys. Rev.* **25**, 753 (1925).
- [51] X. Xing, W. Zhou, J. Wang, Z. Zhu, Y. Zhang, N. Zhou, B. Qian, X. Xu, and Z. Shi, Two-band and pauli-limiting effects on the upper critical field of 112-type iron pnictide superconductors. *Sci. Rep.* **7**, 45943 (2017).
- [52] A. Kononov, Data for “Superconductivity in type-II Weyl-semimetal WTe₂ induced by a normal metal contact”, (Zenodo, 2020). <https://doi.org/10.5281/zenodo.3934679>